Conduction-band and valence-band structures in strained $In_{1-x}Ga_xAs/InP$ quantum wells on (001) InP substrates

Mitsuru Sugawara, Niroh Okazaki, Takuya Fujii, and Susumu Yamazaki
Fujitsu Laboratories Ltd., 10-1 Morinosato-Wakamiya, Atsugi 243-01, Japan
(Received 5 April 1993)

We study conduction-band and valence-band structures in strained $In_{1-x}Ga_xAs/InP$ quantum wells on (001) InP substrates using the $\mathbf{k}\cdot\mathbf{p}$ perturbation approach and magneto-optical absorption measurements. We evaluate the band offset between $In_{1-x}Ga_xAs$ and InP using the tight-binding model. We derive a formula for calculating conduction-band dispersion both in biaxially strained bulk layers and quantum wells from the first-order $\mathbf{k}\cdot\mathbf{p}$ perturbation. We use our formula to show that the electron effective mass of strained $In_{1-x}Ga_xAs$ and strained $In_{1-x}Ga_xAs/InP$ quantum wells are anisotropic, and that the masses depend significantly on the strain and well width. We evaluate magneto-optical absorption spectra of multiple quantum wells with compositions, x, from 0.34 to 0.58, corresponding to about $\pm 1\%$ in-plane strain, and with well widths from 6 to 14 nm. We analyze the diamagnetic shifts of exciton resonances based on the effective-mass equations taking both conduction- and valence-band nonparabolic dispersion into account. We obtain in-plane electron, hole, and reduced effective masses of excitons and Luttinger-Kohn effective-mass parameters for valence bands as a function of composition.

I. INTRODUCTION

The crystal-growth technology of thin-film semiconductor structures has made it possible to incorporate strain into semiconductor devices without generating misfit dislocations.[1,2] The strained quantum wells and strained superlattices changed the conventional thinking that semiconductor epitaxial layers should be lattice matched to substrates, and widened the choice of materials for electronic and optical devices.[3] Another, and stronger, motivation for introducing strain is to design the electronic band structure of materials through changes in the volume and symmetry of the crystal lattice.[4] This kind of band engineering in strained quantum wells has focused primarily on their valence bands. Second-order $\mathbf{k}\cdot\mathbf{p}$ perturbation calculations using Luttinger-Kohn Hamiltonian matrix[5] show that in-plane dispersion of the topmost valence bands is highly nonparabolic because of the mixing between split heavy-hole (HH) and light-hole (LH) subbands at the Γ point.[6–15] Strain in quantum wells can change the splitting energies,[16–18] degree of mixing, in-plane dispersion relationship, and effective masses of valence bands.[19–29]

The most successful example of valence-band engineering in optical devices is strained semiconductor quantum-well lasers, first noted by Yablonovitch[20,22] and Adams;[30] biaxially compressive strain in the well layers reduces intersubband mixing and improves band parabolicity, resulting in a low threshold carrier concentration. This effect was expected not only to reduce threshold current[20–22,30] but also to improve other lasing characteristics such as modulation bandwidth[28] and spectral linewidth.[29] We used a similar theoretical approach to point out that $In_{1-x}Ga_xAs/InP$ quantum-well lasers under a biaxial tensile strain on (001) InP substrates can also have lower threshold currents than lattice-matched ones.[31] Thijs and co-workers showed, in a series of works on strained $In_{1-x}Ga_xAs/In_{1-x}Ga_xAs_yP_{1-y}$ quantum-well lasers on InP substrates,[32–35] that threshold current densities could be made lower by strain in either direction, and demonstrated high output power, high-temperature operation, and a low linewidth enhancement factor.

Note that in-plane band dispersion in strained quantum wells has not been fully established, however. The strain effect on the conduction-band effective mass in quantum wells has received little attention. The valence-band effective-mass parameters (Luttinger-Kohn parameters[5]), to which the detail of the calculated dispersion is markedly sensitive, have not been well verified. These parameters were theoretically calculated by Lawaetz[36] for various III-V and II-VI materials, but few values have been checked by experiments, casting doubt about the numerical details of valence-band dispersion.

This paper reports our study of conduction- and valence-band structures of biaxially strained $In_{1-x}Ga_xAs/InP$ quantum wells on (001) InP substrates. We focused on the conduction-band effective mass and valence-band Luttinger-Kohn parameters. We use the $\mathbf{k}\cdot\mathbf{p}$ perturbation approach to calculate band dispersion, and evaluate magneto-optical absorption spectra to obtain accurate mass parameters. We start by discussing band offsets of this quantum-well system needed for the dispersion calculation, using our tight-binding model including cation d-orbital bases.[37] From the first-order $\mathbf{k}\cdot\mathbf{p}$ perturbation approach, we derive a formula for calculating conduction-band dispersion both in biaxially strained bulk layers and quantum wells. We used our formula to calculate the band-edge electron effective mass of strained $In_{1-x}Ga_xAs$ and $In_{1-x}Ga_xAs/InP$ strained quantum wells. For the valence bands, we use a Luttinger-Kohn 6×6 Hamiltonian matrix.[5] We evaluated the optical-

0163-1829/93/48(11)/8102(17)/$06.00

absorption spectra of $In_{1-x}Ga_xAs/InP$ quantum wells with the composition of $x=0.34-0.58$ and well width of $L_w=6-14$ nm under magnetic fields of up to 8 T perpendicular to the quantum wells. We analyzed the diamagnetic shifts of exciton resonances using effective-mass equations taking both conduction- and valence-band nonparabolic dispersion into account. From our analysis, we obtain in-plane electron, hole, and reduced effective masses of excitons, and Luttinger-Kohn effective-mass parameters for valence bands as a function of crystal composition.

II. BAND OFFSET

Electronic states and optical properties of semiconductor quantum wells, where a thin semiconductor film is sandwiched between different materials via heterojunctions, strongly depend on their confinement potentials formed by the spatial variation of band-edge energies. III-V and II-VI semiconductor materials with zinc-blende crystal lattices have an s-like conduction-band edge and a p-like valence-band edge, topmost HH and LH bands and a split-off band under spin-orbit interaction. We can illustrate the band-edge energies at the heterojunction of A and B semiconductors as shown in Fig. 1. Δ_A and Δ_B are the spin-orbit splitting energies Δ of each material, E_A and E_B are the band gaps, V_s is the offset of the conduction band, V_p is the offset of the topmost valence band, and V_δ is the offset of the split-off band. The definitions of symbols in Fig. 1 are taken from Ref. 38. In multilayer structures, we would expect the energy steps formed by each band to give steplike carrier confinement potentials $V_s(z)$, $V_p(z)$, and $V_\delta(z)$ in the growth direction z. For example, $V_s(z)=0$ when z is in material A and $V_s(z)=V_s$ when z is in material B. Depending on the signs of V_s, V_p, and V_δ, there are several kinds of quantum wells with significantly different electronic and optical properties. Many technologically important III-V semiconductors such as $In_{1-x}Ga_xAs_yP_{1-y}/InP$ (Ref. 39) and $Ga_{1-x}Al_xAs/GaAs$ (Refs. 40 and 41) form a type-I band offset, where $V_s>0$ and $V_p<0$. In biaxially strained

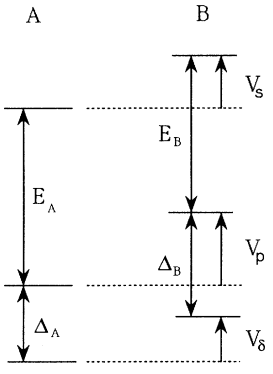

FIG. 1. Band-edge energies at the heterojunction of A and B semiconductors.

$In_{1-x}Ga_xAs/InP$ quantum wells on (001) InP substrates, Cavicchi evaluated conduction-band offset values[42] for compositions of $x=0.31$, 0.47 (lattice-matched to InP), and 0.63 by admittance spectroscopy. We evaluate offset values V_s, V_p, and V_δ of this quantum-well system for the entire range of compositions ($x=0-1$) based on our tight-binding model.[37] We also show band offset of $In_{1-x}Ga_xAs/In_{0.52}Al_{0.48}As$, where $In_{0.52}Al_{0.48}As$ is lattice matched to InP and forms quantum-well barriers.

Our tight-binding model is an improvement of the well-known Harrison's tight-binding model[43,44] in that it incorporates cation d orbitals as basis functions. Harrison's model is quite simple and, at the same time, agrees exceptionally well with experiments in III-V semiconductors. In Harrison's approach, the valence-band offset between two semiconductors is the energy difference between respective valence-band maximums, which is expressed simply as a cation-anion bonding p state. The only, but crucial, exception was that, for heterojunctions with aluminum atoms such as $GaAs/Ga_xAl_{1-x}As$ and $In_{1-y}Ga_yAs/In_{1-x}Al_xAs$, the model predicts an almost zero offset, contradicted by experiments.[43,45] Wei pointed out that this difficulty can be overcome by incorporating cation d orbitals in the tight-binding model;[46,47] repulsion between anion p states and cation d states moves the valence-band maximum upward in GaAs and downward in AlAs, giving a significant valence-band offset (type-I band offset). We solved a 13×13 tight-binding matrix formed by cation s, p, and d orbitals and anion s and p orbitals, assuming crystal-lattice translational symmetry and interaction only between neighboring atoms.

The mixed-state eigenvalues E at $\mathbf{k}=\mathbf{0}$ are given by the third-order equation[37]

$$(\varepsilon_p^a-E)(\varepsilon_p^c-E)(\varepsilon_d^c-E)-(4E_{x,x})^2(\varepsilon_d^c-E) -(4E_{x,yz})^2(\varepsilon_p^c-E)=0\ , \quad (1)$$

where ε_p^a is the anion p-state energy, ε_p^c is the cation p-state energy, ε_d^c is the cation d-state energy, and $E_{x,x}$ and $E_{x,yz}$ are the interatomic matrix elements of zinc-blende crystals (Appendix A). The bonding p-state energy (valence-band maximum $E_{v,0}$) is the middle eigenvalue of Eq. (1) when the order of atomic energy levels is $\varepsilon_p^a>\varepsilon_d^c$, and is the smallest one when $\varepsilon_d^c>\varepsilon_p^a$. The p-d repulsion gives rise to the upward (downward) energy shift of the bonding p state and the downward (upward) energy shift of the d state when $\varepsilon_p^a>\varepsilon_d^c(\varepsilon_d^c>\varepsilon_p^a)$. Note that, if we neglect the p-d coupling, i.e., $E_{x,yz}=0$, Eq. (1) reduces to the Harrison's well-known equation:[43,44]

$$E=\frac{\varepsilon_p^c+\varepsilon_p^a}{2}\pm\left\{\left[\frac{\varepsilon_p^c-\varepsilon_p^a}{2}\right]^2+(4E_{x,x})^2\right\}^{1/2}\ . \quad (2)$$

The larger eigenvalue represents the antibonding p state and the smaller one is for the bonding p state.

Biaxial strain and spin-orbit interaction shift and split the degenerate valence-band maximum. By adding E_{HH}, E_{LH}, and E_{SO}, which include phenomenological deformation potentials and spin-orbit splitting energy (Appendix B) to $E_{v,0}$, we obtain the energies of HH, LH, and split-off

(SO) valence bands:

$$E_{v,0}^{\mathrm{HH}} = E_{v,0} + E_{\mathrm{HH}} , \quad (3)$$

$$E_{v,0}^{\mathrm{LH}} = E_{v,0} + E_{\mathrm{LH}} , \quad (4)$$

and

$$E_{v,0}^{\mathrm{SO}} = E_{v,0} + E_{\mathrm{SO}} . \quad (5)$$

The conduction-band-edge energy at $\mathbf{k}=\mathbf{0}$, $E_{c,0}^{s}$, is estimated using E_0 (the band gap for direct semiconductors) as

$$E_{c,0}^{s} = E_{c,0} + P_{\varepsilon}^{c} = E_{v,0} + E_0 + P_{\varepsilon}^{c} , \quad (6)$$

where P_{ε}^{c} is the energy shift due to hydrostatic deformation (Appendix B).

From Eqs. (1) and (3)–(6), we calculated the conduction- and valence-band-edge energies of $In_{1-x}Ga_xAs$, InP, and $In_{0.52}Al_{0.48}As$ with $\mathbf{k}=\mathbf{0}$ direct gaps. First, we calculated $E_{v,0}$ and $E_{c,0}$ of the constituent binary materials. We then calculated those of alloys by interpolation, taking bowing parameters into account. We then added terms for strain and spin-orbit interaction. Input parameters for calculating the interatomic matrix elements (Appendix A) are lattice constants, atomic orbital energies, and d-orbital radius. We took p-state atomic-orbital energies from Harrison's table[48] as $\varepsilon_p^a = -8.33$ eV for P and -7.91 eV for As, and $\varepsilon_p^c = -4.86$ eV for Al, -4.90 eV for Ga, and -4.69 eV for In. The problem with this approach is that reliable d-orbital data are difficult to obtain. For both In and Ga, we used $\varepsilon_d^c = -21.5$ eV, which we estimated from the calculated values of ε_p^a-ε_d^c in Table IV of Ref. 47. We substituted $\varepsilon_d^c = 0$ for Al, whose $3d$ orbitals are empty. We assume $r_d = 1$ Å for all materials. For valence-band bowing parameters, we halved the bowing parameters of the E_0 gap listed in Ref 49: 0.6 eV for $In_{1-x}Ga_xAs$ and 0.24 eV for $In_{1-x}Al_xAs$. Other parameters used in the calculation are listed in Table I. The lattice constant of AlAs is 5.6611 Å.

Figure 2(a) shows the band-edge energies at $\mathbf{k}=\mathbf{0}$ for free-standing (unstrained) $In_{1-x}Ga_xAs$ as a function of gallium composition x. As x increases, the conduction-band energy increases monotonically and the valence-band energy decreases. The horizontal dashed lines at the longitudinal axes are band edges of InP, and offsets (V_S, V_p, and V_δ) are shown by arrows. V_S is positive at

TABLE I. Band gap E_0, lattice constant a_0, elastic stiffness constants C_{11} and C_{12}, deformation potentials a_s and b_s, conduction-band-edge effective mass m_{Γ_6}, and the spin-orbit-splitting energy Δ. l.i. stands for linear interpolation.

Parameters	InAs	GaAs	InP	$In_{1-x}Ga_xAs$
E_0 (eV)	0.36	1.43	1.35	$0.36+0.624x+0.446x^2$
a_0 (Å)	6.0584	5.6533	5.8687	l.i.
$C_{11}(\times 10^{11}$ dyn/cm^2)	8.329	11.88		$C_{11}(x)$[a]
$C_{12}(\times 10^{11}$ dyn/cm^2)	4.526	5.38		$C_{12}(x)$[b]
a_s (eV)	−6.0	−8.46		l.i.
b_s (eV)	−1.8	−1.7		l.i.
m_{Γ_6}/m_0	0.023	0.067		l.i.
Δ (eV)	0.4	0.34	0.1	l.i.

[a] $C_{11}(x) = [(1-x)a_0(\mathrm{InAs})C_{11}(\mathrm{InAs}) + xa_0(\mathrm{GaAs})C_{11}(\mathrm{GaAs})]/a_0(x)$.

[b] $C_{12}(x) = [(1-x)a_0(\mathrm{InAs})C_{12}(\mathrm{InAs}) + xa_0(\mathrm{GaAs})C_{12}(\mathrm{GaAs})]/a_0(x)$.

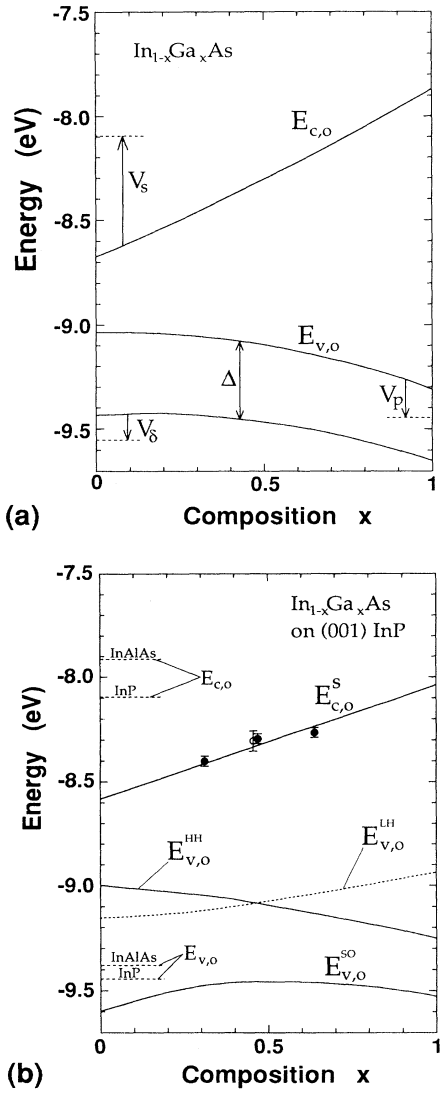

FIG. 2. (a) Conduction-band minimum $E_{c,0}$, valence-band maximum $E_{v,0}$, and split-off band edge with the spin-orbit splitting energy of Δ in free-standing $In_{1-x}Ga_xAs$. Horizontal dashed lines are the band edges of InP. The offsets of each band against InP are V_s, V_p, and V_δ. (b) Band-edge energies of the conduction-band, $E_{c,0}^{s}$; the HH band, $E_{v,0}^{\mathrm{HH}}$; the LH band, $E_{v,0}^{\mathrm{LH}}$; and the split-off band, $E_{v,0}^{\mathrm{SO}}$ in biaxially strained $In_{1-x}Ga_xAs$ on (001) InP substrates. $E_{c,0}$ and $E_{v,0}$ of InP and $In_{0.52}Al_{0.48}As$ lattice matched to InP are also shown by horizontal dashed lines.

$x=0-0.75$, V_δ is negative at $x=0-0.78$, and V_p is negative at all compositions.

Figure 2(b) is shown assuming that $In_{1-x}Ga_xAs$ layers are grown coherently on (001) InP substrates and under biaxial strain. The topmost valence band splits into HH and LH states, and the conduction-band edge is less dependent on composition. For both InP and $In_{0.52}Al_{0.48}As$, $E_{c,0}$ and $E_{v,0}$ are shown by dashed horizontal lines at the longitudinal axis. Solid circles represent the conduction-band edge measured by admittance spectroscopy (they are plotted from the InP conduction-band edge),[42] and an open circle measured by capacitance-voltage profiling (plotted from the $In_{0.52}Al_{0.48}As$ conduction-band edge),[50] showing a good agreement with calculations. In $In_{1-x}Ga_xAs/InP$ quantum wells, the transition from a type-I to a type-II potential profile occurs at $x=0.9$. This type transition has been seen in the optical-absorption spectra of this strained quantum-well system, although the transition occurred at the slightly smaller composition: $x=0.78-0.85$.[51] $In_{1-x}Ga_xAs/In_{0.52}Al_{0.48}As$ quantum wells are expected to have a type-I potential profile at any composition because $In_{0.52}Al_{0.48}As$ has a higher conduction-band edge than InP.

III. CONDUCTION BAND

We use the first-order $\mathbf{k}\cdot\mathbf{p}$ perturbation approach to describe the conduction band in biaxially strained quantum wells grown on (001) substrates. For quantum wells of zinc-blende III-V and II-VI materials, with a fundamental band gap at the Γ point, the effective-mass approximation gives the wave function as[38]

$$\Phi=\sqrt{\Omega/D}\,e^{i\mathbf{k}_\parallel\cdot\mathbf{r}}\sum_{j=1}^{8}\varphi_n^j(z,\mathbf{k}_\parallel)u_0^j\ , \tag{7}$$

where Ω is the unit-cell volume, D is the area of quantum wells, $\mathbf{k}_\parallel$ is the in-plane wave vectors, $\mathbf{r}$ is the in-plane coordinate vectors, z is the coordinate perpendicular to quantum-well layers, and $\varphi_n^j(z,\mathbf{k}_\parallel)$ is the envelope wave function representing a confined state with a quantum number n. The periodic parts of band-edge Bloch functions, u_0^j, are assumed to be the same in well and barrier layers. We take[52,53]

$$|S\uparrow\rangle,\quad |S\downarrow\rangle\ , \tag{8}$$

$$|\tfrac{3}{2},\tfrac{3}{2}\rangle=\frac{1}{\sqrt{2}}|(X+iY)\uparrow\rangle\ , \tag{9}$$

$$|\tfrac{3}{2},-\tfrac{3}{2}\rangle=-\frac{1}{\sqrt{2}}|(X-iY)\downarrow\rangle\ , \tag{10}$$

$$|\tfrac{3}{2},\tfrac{1}{2}\rangle=\frac{1}{\sqrt{6}}|(X+iY)\downarrow-2Z\uparrow\rangle\ , \tag{11}$$

$$|\tfrac{3}{2},-\tfrac{1}{2}\rangle=-\frac{1}{\sqrt{6}}|(X-iY)\uparrow+2Z\downarrow\rangle\ , \tag{12}$$

$$|\tfrac{1}{2},\tfrac{1}{2}\rangle=\frac{1}{\sqrt{3}}|(X+iY)\downarrow+Z\uparrow\rangle\ , \tag{13}$$

and

$$|\tfrac{1}{2},-\tfrac{1}{2}\rangle=\frac{1}{\sqrt{3}}|(X-iY)\uparrow-Z\downarrow\rangle\ , \tag{14}$$

where $\uparrow$ and $\downarrow$ are spin functions, S has atomic s-orbital symmetry and X, Y, and Z have p-orbital symmetry. The quantization axis of the angular momenta is taken in the $\langle 001\rangle$ direction, the z direction. P-state bases of Eqs. (9)–(14), written in the (J,M_J) representation, are taken to diagonalize the spin-orbit interaction. S states are the major part of the conduction band, $|\frac{3}{2},\pm\frac{3}{2}\rangle$ and $|\frac{3}{2},\pm\frac{1}{2}\rangle$ states are HH and LH topmost valence bands, and $|\frac{1}{2},\pm\frac{1}{2}\rangle$ states are the split-off band. (We incorporate the effect of d orbitals only in the band-edge energies of the $\mathbf{k}\cdot\mathbf{p}$-matrix diagonal terms, i.e., confinement potentials.) Kane's $\mathbf{k}\cdot\mathbf{p}$ perturbation approach revealed that, in bulk semiconductor materials, effective mass and nonparabolic dispersion of the conduction band originate from the first-order interactions between s- and p-state bases.[52] Bastard[38] solved the first-order $\mathbf{k}\cdot\mathbf{p}$ matrix in direct-gap semiconductor quantum wells and showed that the in-plane electron effective mass is greater than the bulk band-edge mass, m_{Γ_6}. This enhancement is caused by the increase in the quantized electron energy level in the nonparabolic conduction band.

We include the effect of biaxial strain on the $\mathbf{k}\cdot\mathbf{p}$ coupling. For quantum wells grown coherently on (001) substrates and under biaxial strain, we use a new set of bases to diagonalize the strain Hamiltonian:

$$f_s^+=|S\uparrow\rangle,\quad f_s^-=|S\downarrow\rangle\ , \tag{15}$$

$$f_{\rm HH}^{\pm}=|\tfrac{3}{2},\pm\tfrac{3}{2}\rangle\ , \tag{16}$$

$$f_{\rm LH}^{\pm}=\alpha|\tfrac{3}{2},\pm\tfrac{1}{2}\rangle+\beta|\tfrac{1}{2},\pm\tfrac{1}{2}\rangle\ , \tag{17}$$

and

$$f_{\rm SO}^{\pm}=-\beta|\tfrac{3}{2},\pm\tfrac{1}{2}\rangle+\alpha|\tfrac{1}{2},\pm\tfrac{1}{2}\rangle\ , \tag{18}$$

where α and β represent the degree of mixing between $|\frac{3}{2},\pm\frac{1}{2}\rangle$ and $|\frac{1}{2},\pm\frac{1}{2}\rangle$ states[54,55] (Appendix B). With no strain, $\alpha=1$ and $\beta=0$. With strain, α decreases and β increases under the normalizing condition that $|\alpha|^2+|\beta|^2=1$. Then, taking the conduction-band edge as the energy origin, the 8×8 first-order $\mathbf{k}\cdot\mathbf{p}$ matrix is given as Eq. (19), where $k_\pm=(k_x\pm ik_y)/\sqrt{2}$, and $\mathbf{k}_\parallel=(k_x,k_y)$ is the in-plane wave vector. When $|z|\le L_w/2$ (L_w is the well width), $V_s(z)=V_p(z)=V_\delta(z)=0$. When $|z|>L_w/2$, $V_s(z)=V_s$, $V_p(z)=V_p$, and $V_\delta(z)=V_\delta$. We assume flat-band quantum wells with no applied electric field and intentional doping. When barrier layers are lattice matched to the substrates, $In_{1-x}Ga_xAs/InP$ on (001) InP, for example, $E_c(z)=P_\varepsilon^c$, $E_{\rm HH}(z)=E_{\rm HH}$, $E_{\rm LH}(z)=E_{\rm LH}$, and $E_{\rm SO}(z)=E_{\rm SO}$ when $|z|\le L_w/2$, and $E_c(z)=E_{\rm HH}(z)=E_{\rm LH}(z)=0$ and $E_{\rm SO}(z)=-\Delta_A$ when $|z|>L_w/2$ (Appendix B). The momentum matrix element P is defined as

$$P=\langle S|p_j|j\rangle/m_0\quad (j=X,Y,\text{ and }Z)\ . \tag{20}$$

We omitted the free-electron term $(\hbar^2/2m_0)(k_\parallel^2+k_z^2)$ from the diagonal matrix elements. The wave vector in

the z direction, k_z, is replaced with $-i\,\partial/\partial z$. The effect of strain is included through α and β in nondiagonal terms and band-edge energies in diagonal terms.

Equation (19) shows that the matrix elements between the p-state bases remain only in the diagonal terms and that they consist only of energy terms. This simplicity enables us to fold an 8×8 matrix to 2×2 for two s-state bases as

$$\begin{bmatrix} H_d & H_n \\ H_n^* & H_d \end{bmatrix}\begin{bmatrix} \varphi_s^+ \\ \varphi_s^- \end{bmatrix}=E\begin{bmatrix} \varphi_s^+ \\ \varphi_s^- \end{bmatrix}, \tag{21}$$

where φ_s^+ and φ_s^- are the envelope wave functions of the S-state bases,

$$H_d=\frac{P^2}{3}\left\{p_z\left[\frac{(\sqrt{2}\alpha-\beta)^2}{E_A-V_p(z)-E_{\rm LH}(z)+E}+\frac{(\sqrt{2}\beta+\alpha)^2}{E_A-V_\delta(z)-E_{\rm SO}(z)+E}\right]p_z+\frac{k_\parallel^2\hbar^2}{2}\left[\frac{3}{E_A-V_p(z)-E_{\rm HH}(z)+E}+\frac{(\alpha-\sqrt{2}\beta)^2}{E_A-V_p(z)-E_{\rm LH}(z)+E}+\frac{(\beta+\sqrt{2}\alpha)^2}{E_A-V_\delta(z)-E_{\rm SO}(z)+E}\right]\right\}+V_s(z)+E_c(z)\,, \tag{22}$$

$$H_n=\frac{P^2\hbar}{3}k_-\left\{\left[\frac{\sqrt{2}\alpha^2-\alpha\beta-\sqrt{2}\beta^2}{E_A-V_p(z)-E_{\rm LH}(z)+E}p_z-p_z\frac{\sqrt{2}\alpha^2+\alpha\beta-\sqrt{2}\beta^2}{E_A-V_p(z)-E_{\rm LH}(z)+E}\right]-\left[\frac{\sqrt{2}\alpha^2-\alpha\beta-\sqrt{2}\beta^2}{E_A-V_\delta(z)-E_{\rm SO}(z)+E}p_z-p_z\frac{\sqrt{2}\alpha^2+\alpha\beta-\sqrt{2}\beta^2}{E_A-V_\delta(z)-E_{\rm SO}(z)+E}\right]\right\}, \tag{23}$$

and $p_z=\hbar k_z$.

The equations above can be applied to the problem on bulk materials under biaxial strain by neglecting the position dependence of $\varphi_s^\pm$, replacing $E_c(z)$, $E_{\rm HH}(z)$, $E_{\rm LH}(z)$, and $E_{\rm SO}(z)$ with P_ε^c, $E_{\rm HH}$, $E_{\rm LH}$, and $E_{\rm SO}$, respectively, and omitting confinement potentials in Eqs. (22) and (23). The dispersion relationship is then given by finding numerically the eigenvalues of the 2×2 matrix against wave vectors. In the $k_\parallel$ and k_z directions, the nondiagonal terms exactly vanish and we have an analytical expression for band-edge effective mass from the diagonal terms with $E=P_\varepsilon^c$ substituted in the denominators:[4]

$$1/m_e^\parallel=(1+D')/m_0+\frac{P^2}{3}\left[\frac{3}{E_A+P_\varepsilon^c-E_{\rm HH}}+\frac{(\alpha-\sqrt{2}\beta)^2}{E_A+P_\varepsilon^c-E_{\rm LH}}+\frac{(\beta+\sqrt{2}\alpha)^2}{E_A+P_\varepsilon^c-E_{\rm SO}}\right] \tag{24}$$

in the $k_\parallel$ direction (in-plane direction), and

$$1/m_e^\perp=(1+D')/m_0+\frac{2P^2}{3}\left[\frac{(\sqrt{2}\alpha-\beta)^2}{E_A+P_\varepsilon^c-E_{\rm LH}}+\frac{(\sqrt{2}\beta+\alpha)^2}{E_A+P_\varepsilon^c-E_{\rm SO}}\right] \tag{25}$$

in the k_z direction (perpendicular to epitaxial layers). Note that a free-electron term and a second-order $\mathbf{k}\cdot\mathbf{p}$ perturbation term D' have been added. The denominators are the optical transition energies from each valence band to the conduction band. The momentum matrix element is related to the conduction-band-edge effective mass, m_{Γ_6}, with no strain [substituting $\alpha=1$, $\beta=0$, $P_\varepsilon^c=E_{\rm HH}=E_{\rm LH}=0$, and $E_{\rm SO}=-\Delta_A$ in Eq. (24) or (25)] by the equation

$$P^2=\frac{1}{2}\left[\frac{1}{m_{\Gamma_6}}-\frac{1+D'}{m_0}\right]\frac{E_A(E_A+\Delta_A)}{E_A+\frac{2}{3}\Delta_A}\,. \tag{26}$$

Assuming that the momentum matrix element is independent of strain, we can estimate the effective masses in strained materials from m_{Γ_6}. In Sec. V, we evaluate P^2 and D' for $In_{1-x}Ga_xAs/InP$ strained quantum wells on (001) InP substrates using a magnetic-field dependence of exciton resonance strength. We find that Eq. (26) gives measured matrix elements with $D'=-6$ for both lattice-matched and biaxially compressive quantum wells, independent of strain. This result supports the assumption above.

The boundary conditions for solving Eq. (21) for quantum wells are that

$$\begin{bmatrix} \varphi_s^+ \\ \varphi_s^- \end{bmatrix}\ \text{and}\ \begin{bmatrix} -\frac{1}{\mu}\frac{\partial}{\partial z} & i\sqrt{2}k_-\eta \\ -i\sqrt{2}k_+\eta & -\frac{1}{\mu}\frac{\partial}{\partial z} \end{bmatrix}\begin{bmatrix} \varphi_s^+ \\ \varphi_s^- \end{bmatrix} \tag{27}$$

are continuous,[38] where

$$\mu^{-1}=\frac{2P^2}{3}\left[\frac{(\sqrt{2}\alpha-\beta)^2}{E_A-V_p(z)-E_{\rm LH}(z)+E}+\frac{(\sqrt{2}\beta+\alpha)^2}{E_A-V_\delta(z)-E_{\rm SO}(z)+E}\right] \tag{28}$$

and

$$
\begin{array}{c|cccccc}
 & f_s^+ & f_{\mathrm{HH}}^+ & f_{\mathrm{LH}}^+ & f_{\mathrm{SO}}^+ & f_S^- & f_{\mathrm{HH}}^- \\
f_s^+ & V_s(z)+E_c(z) & P\hbar k_+ & \left[-\sqrt{\frac{2}{3}}\alpha+\frac{\beta}{\sqrt{3}}\right]P\hbar k_z & \left[\sqrt{\frac{2}{3}}\beta+\frac{\alpha}{\sqrt{3}}\right]P\hbar k_z & 0 & 0 \\
f_{\mathrm{HH}}^+ & P\hbar k_- & -E_A+V_P(z)+E_{\mathrm{HH}}(z) & 0 & 0 & \left[\frac{\alpha}{\sqrt{3}}+\sqrt{\frac{2}{3}}\beta\right]P\hbar k_- & 0 \\
f_{\mathrm{LH}}^+ & \left[-\sqrt{\frac{2}{3}}\alpha+\frac{\beta}{\sqrt{3}}\right]P\hbar k_z & 0 & -E_A+V_P(z)+E_{\mathrm{LH}}(z) & 0 & \left[-\frac{\beta}{\sqrt{3}}+\sqrt{\frac{2}{3}}\alpha\right]P\hbar k_- & 0 \\
f_{\mathrm{SO}}^+ & \left[\sqrt{\frac{2}{3}}\beta+\frac{\alpha}{\sqrt{3}}\right]P\hbar k_z & 0 & 0 & -E_A+V_\delta(z)+E_{\mathrm{SO}}(z) & 0 & 0 \\
f_S^- & 0 & 0 & \left[\frac{\alpha}{\sqrt{3}}+\sqrt{\frac{2}{3}}\beta\right]P\hbar k_- & \left[-\frac{\beta}{\sqrt{3}}+\sqrt{\frac{2}{3}}\alpha\right]P\hbar k_- & V_s(z)+E_c(z) & -P\hbar k_- \\
f_{\mathrm{HH}}^- & 0 & 0 & 0 & 0 & -P\hbar k_+ & -E_A+V_P(z)+E_{\mathrm{HH}}(z) \\
f_{\mathrm{LH}}^- & \left[-\frac{\alpha}{\sqrt{3}}+\sqrt{\frac{2}{3}}\beta\right]P\hbar k_- & 0 & 0 & 0 & \left[-\sqrt{\frac{2}{3}}\alpha-\frac{\beta}{\sqrt{3}}\right]P\hbar k_z & 0 \\
f_{\mathrm{SO}}^- & \left[\frac{\beta}{\sqrt{3}}+\sqrt{\frac{2}{3}}\alpha\right]P\hbar k_- & 0 & 0 & 0 & \left[\sqrt{\frac{2}{3}}\beta-\frac{\alpha}{\sqrt{3}}\right]P\hbar k_z & 0
\end{array}
\begin{array}{c|cccc}
 & f_{\mathrm{LH}}^- & f_{\mathrm{SO}}^- \\
f_s^+ & 0 & 0 \\
f_{\mathrm{HH}}^+ & 0 & 0 \\
f_{\mathrm{LH}}^+ & 0 & 0 \\
f_{\mathrm{SO}}^+ & 0 & 0 \\
f_S^- & \left[-\frac{\alpha}{\sqrt{3}}+\sqrt{\frac{2}{3}}\beta\right]P\hbar k_- & \left[\frac{\beta}{\sqrt{3}}+\sqrt{\frac{2}{3}}\alpha\right]P\hbar k_- \\
f_{\mathrm{HH}}^- & 0 & 0 \\
f_{\mathrm{LH}}^- & -E_A+V_P(z)+E_{\mathrm{LH}}(z) & 0 \\
f_{\mathrm{SO}}^- & 0 & -E_A+V_\delta(z)+E_{\mathrm{SO}}(z)
\end{array}
\tag{19}
$$

$$
\eta=\frac{\sqrt{2}(\sqrt{2}\alpha^2+\alpha\beta-\sqrt{2}\beta^2)P^2}{3}\times\left[\frac{1}{E_A-V_p(z)-E_{\mathrm{LH}}(z)+E}-\frac{1}{E_A-V_\delta(z)-E_{\mathrm{SO}}(z)+E}\right]. \tag{29}
$$

Bastard derived an analytical eigenvalue equation from Eq. (21) to give the conduction-band energy in unstrained quantum wells.[38] Since H_d is even and H_n is odd in the z coordinate, there exist two sets of bound-state eigenfunctions with definite parity: even (odd) φ_s^+ and odd (even) φ_s^-. In unstrained quantum wells with $\alpha=1$ and $\beta=0$, the nondiagonal terms [Eq. (23)] in the 2×2 matrix van-

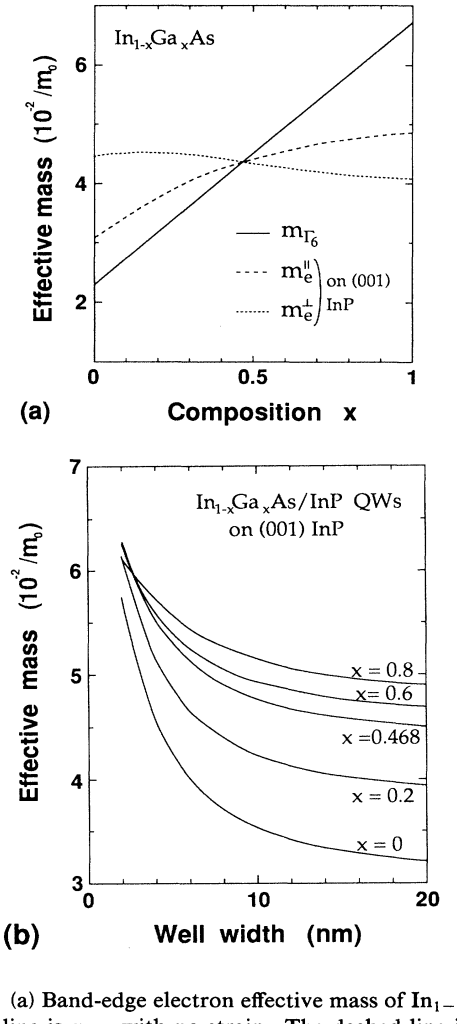

FIG. 3. (a) Band-edge electron effective mass of $In_{1-x}Ga_xAs$. The solid line is m_{Γ_6} with no strain. The dashed line is the in-plane mass [$m_e^{\parallel}$ calculated by Eq. (24)], and the dotted line is the mass perpendicular to layers [$m_e^{\perp}$ calculated by Eq. (25)] for biaxially strained $In_{1-x}Ga_xAs$ on (001) InP substrates. (b) Band-edge in-plane electron effective mass as a function of well width for biaxially strained $In_{1-x}Ga_xAs$/InP quantum wells on (001) InP substrates.

ish in both the well and barrier layers under the flat-band condition. In strained quantum wells, nondiagonal terms exactly vanish only at the band edge ($k_{-}=0$). Also, at nonzero wave vectors, we neglect the nondiagonal terms as long as $H_d \gg H_n$. This assumption holds well near band edges ($k_{-}\cong 0$) or under small strains ($\alpha\cong 1$ and $\beta\cong 0$). When H_n is of the same order as H_d, we must numerically solve the 2×2 matrix. If we let $H_n=0$, we have only to replace parameters in Bastard's equation as

$$\cos k_A L_w + \frac{1}{2}\left[\frac{\kappa_B\mu_A}{\mu_B k_A}-\frac{k_A\mu_B}{\mu_A\kappa_B}-\frac{k_{\parallel}^2(\eta_A-\eta_B)^2}{\kappa_B k_A \mu_A^{-1}\mu_B^{-1}}\right]\times\sin k_A L_w = 0 , \quad (30)$$

where

$$k_A^2=\left\{\frac{3(E-P_{\varepsilon}^c)}{P^2\hbar^2}-\frac{k_{\parallel}^2}{2}\left[\frac{3}{E_A-E_{\rm HH}+E}+\frac{(\alpha-\sqrt{2}\beta)^2}{E_A-E_{\rm LH}+E}+\frac{(\beta+\sqrt{2}\alpha)^2}{E_A-E_{\rm SO}+E}\right]\right\}\left[\frac{(\sqrt{2}\alpha-\beta)^2}{E_A-E_{\rm LH}+E}+\frac{(\sqrt{2}\beta+\alpha)^2}{E_A-E_{\rm SO}+E}\right]^{-1}, \quad (31)$$

$$\kappa_B^2=\left\{\frac{k_{\parallel}^2}{2}\left[\frac{3+(\alpha-\sqrt{2}\beta)^2}{E_A-V_p+E}+\frac{(\beta+\sqrt{2}\alpha)^2}{E_A+\Delta_A-V_\delta+E}\right]-\frac{3(E-V_s)}{P^2\hbar^2}\right\}\left[\frac{(\sqrt{2}\alpha-\beta)^2}{E_A-V_p+E}+\frac{(\sqrt{2}\beta+\alpha)^2}{E_A+\Delta_A-V_\delta+E}\right]^{-1}, \quad (32)$$

and μ_A, μ_B, η_A, and η_B are the values of $\mu(z)$ and $\eta(z)$ in the well and barrier layers, respectively. The roots of Eq. (30) give confined-state subband energies in the form of

$$E_{c,n}=E_{c,n}^z+E_{c,n}^{\parallel}(\mathbf{k}_{\parallel}) . \quad (33)$$

We calculated band-edge electron effective masses of $In_{1-x}Ga_xAs$ as a function of the composition, x [Fig. 3(a)]. Material parameters needed for the calculation are listed in Table I. The solid line represents m_{Γ_6} in unstrained $In_{1-x}Ga_xAs$ given by the linear interpolation between InAs and GaAs, neglecting bowing. The dashed line is for $m_e^{\parallel}$ [Eq. (24)] and the dotted line is for $m_e^{\perp}$ [Eq. (25)] in biaxially strained $In_{1-x}Ga_xAs$ on (001) InP substrates. We assumed that the momentum matrix element is independent of strain, and neglected the contribution of the second-order perturbation ($D'=0$). (If we use $D'=-6$ determined from the exciton resonance strength in Sec. V, the result is modified by 10% at most.) The mass drops drastically under biaxial tensile strain ($x>0.467$), and increases under biaxial compressive strain ($x<0.467$), primarily due to the strain-induced change in the energy difference between each valence and conduction band. Note that the mass shows anisotropy; $m_{\Gamma_6}>m_e^{\parallel}>m_e^{\perp}$ under biaxially tensile strain ($x>0.468$), and $m_{\Gamma_6}<m_e^{\parallel}<m_e^{\perp}$ under biaxially compressive strain ($x<0.468$).

We calculated the in-plane ground-state ($n=1$) electron effective mass at the band edge using the second derivative of $E_{c,n}^{\parallel}(\mathbf{k}_{\parallel})$ as a function of well width in biaxially strained $In_{1-x}Ga_xAs/InP$ quantum wells on (001) InP substrates [Fig. 3(b)]. V_s, V_p, and V_δ are taken from Fig. 2(a). As the well width decreases, the mass increases monotonically due to the nonparabolic characteristics of conduction-band dispersion. Note that, in 2-nm quantum wells, the mass increases by a few tens to two hundred percent from the bulk band-edge mass.

IV. VALENCE BAND

It is well known that the heavy-hole effective mass does not originate from the direct $\mathbf{k}\cdot\mathbf{p}$ coupling in Eq. (19), but arises from the indirect second-order $\mathbf{k}\cdot\mathbf{p}$ coupling between p-state bases due to virtual transitions to more remote band edges.[5,52,53] The second-order $\mathbf{k}\cdot\mathbf{p}$ matrix with the six p-state band-edge bases of Eqs. (9)–(14) is known as the Luttinger-Kohn 6×6 matrix.[5] Many works have attempted to calculate the in-plane valence-band dispersion in quantum wells,[6–15,19–29] especially $GaAs/Al_xGa_{1-x}As$ and $In_{1-x}Ga_xAs/InP$ systems. These studies clarified the significant valence-band nonparabolic characteristics under intersubband mixing, and the effect of strain on dispersion. Taking the z direction as the quantization axis of angular momenta, the matrix is[5]

$$H_{\rm LK}(\mathbf{k})=-\begin{array}{c} \begin{matrix} \left|\frac{3}{2},\frac{3}{2}\right\rangle & \left|\frac{3}{2},\frac{1}{2}\right\rangle & \left|\frac{3}{2},-\frac{1}{2}\right\rangle & \left|\frac{3}{2},-\frac{3}{2}\right\rangle & \left|\frac{1}{2},\frac{1}{2}\right\rangle & \left|\frac{1}{2},-\frac{1}{2}\right\rangle \end{matrix} \\ \begin{bmatrix} P_k+Q_k & -S_k & R_k & 0 & \frac{1}{\sqrt{2}}S_k & -\sqrt{2}R_k \\ -S_k^* & P_k-Q_k & 0 & R_k & \sqrt{2}Q_k & -\sqrt{\frac{3}{2}}S_k \\ R_k^* & 0 & P_k-Q_k & S_k & -\sqrt{\frac{3}{2}}S_k^* & -\sqrt{2}Q_k \\ 0 & R_k^* & S_k^* & P_k+Q_k & \sqrt{2}R_k^* & \frac{1}{\sqrt{2}}S_k^* \\ \frac{1}{\sqrt{2}}S_k^* & \sqrt{2}Q_k & -\sqrt{\frac{3}{2}}S_k & \sqrt{2}R_k & P_k+\Delta & 0 \\ -\sqrt{2}R_k^* & -\sqrt{\frac{3}{2}}S_k^* & -\sqrt{2}Q_k & \frac{1}{\sqrt{2}}S_k & 0 & P_k+\Delta \end{bmatrix} \end{array} , \quad (34)$$

where

$$P_k=\frac{\hbar^2}{2m_0}\gamma_1(k_x^2+k_y^2+k_z^2)\ , \tag{35}$$

$$Q_k=\frac{\hbar^2}{2m_0}\gamma_2(k_x^2+k_y^2-2k_z^2)\ , \tag{36}$$

$$S_k=\frac{\sqrt{3}\hbar^2}{m_0}[\gamma_3 k_z(k_x-ik_\gamma)]\ , \tag{37}$$

$$R_k=\frac{\sqrt{3}\hbar^2}{2m_0}[-\gamma_2(k_x^2-k_y^2)+2i\gamma_3 k_x k_y]\ , \tag{38}$$

and γ_1, γ_2, and γ_3 are Luttinger-Kohn effective-mass parameters. The notation for each matrix element (P, Q, R, and S) is from Ref. 27. We took the topmost valence-band edge as the energy origin. The wave vector perpendicular to quantum-well layers, k_z, is replaced by $-id/dz$.

In (001) strained quantum wells, the effective-mass equation is given by

$$[H_{\rm LK}+H_\varepsilon+V_j(z)I_{6\times6}]\varphi_{6\times1}=E_{v,n}\varphi_{6\times1}\ , \tag{39}$$

where H_ε is the strain Hamiltonian matrix under biaxial strain (Appendix B), $V_j(z)$ is the confinement potentials ($j=p$ for $J=\frac{3}{2}$ bases and $j=\delta$ for $J=\frac{1}{2}$ bases), $I_{6\times6}$ is the 6×6 unit matrix, and $\varphi_{6\times1}$ is a row vector with components $\varphi_n^j(z,\mathbf{k}_\parallel)$. The eigenvalues are given in the form of

$$E_{v,n}=E_{v,n}^z+E_{v,n}^\parallel(\mathbf{k}_\parallel)\ . \tag{40}$$

The 6×6 matrix of Eq. (39) can be separated into two equivalent 3×3 matrices by a unitary transformation[27,56,57] when $\theta_R=2\theta_S+m\pi$, where θ_R is the declination of complex R_k+R_ε, θ_S is that of complex S_k+S_ε, and m is an integer. This condition can be satisfied at any wave vector without shear deformation ($S_\varepsilon=R_\varepsilon=0$) and under axial approximation, i.e. γ_2 and γ_3 replaced with their arithmetic average $\bar\gamma$ in R_k. Boundary conditions in this case are that $\varphi_{3\times1}$ and $M_{3\times3}\varphi_{3\times1}$ are continuous at interfaces,[9,27] where $\varphi_{3\times1}$ is a row vector for transformed bases and $M_{3\times3}$ is the matrix obtained by integrating the unitary-transformed Luttinger-Kohn Hamiltonian across the interfaces.

We numerically calculate in-plane valence-subband dispersion of biaxially strained quantum wells using the differential method with the following approximations. First, we replace γ_2 and γ_3 with $\bar\gamma$ for all matrix elements. The physical implication is neglecting warping and assuming completely spherical dispersion in the bulk valence band. (Since we determine sets of γ_1 and $\bar\gamma$ from the HH and LH splitting energy in Sec. V, γ_2 is substituted for γ_3 in substance.) Dispersion calculated with this spherical approximation or axial approximation (neglecting only in-plane anisotropy) keeps essential band structures under intersubband mixing.[12,56–59] Second, we used common Luttinger-Kohn parameters for both well and barrier layers. This is also a good approximation in type-I quantum wells such as $In_{0.53}Ga_{0.47}As/InP$, as long as well and barrier layers are relatively thick and eigenstates are well localized in well layers. By the latter approximation, the boundary conditions are automatically satisfied in the diagonalization.

The problem with calculating valence-subband dispersion is, as we pointed out in Sec. I, the uncertainty of Luttinger-Kohn parameters. Lawaetz[36] calculated these parameters for a wide variety of III-V and II-VI semiconductors. From Table II of Ref. 36, we see $\gamma_1=19.67$, $\gamma_2=8.37$, $\gamma_3=9.29$, and $\bar\gamma=(\gamma_2+\gamma_3)/2=8.83$ in InAs, and $\gamma_1=7.65$, $\gamma_2=2.41$, $\gamma_3=3.28$, and $\bar\gamma=2.85$ in GaAs. We next determine a set of Luttinger-Kohn parameters γ_1 and $\bar\gamma$, which properly explain optical-absorption spectra of strained quantum wells under a magnetic field. We will calculate the valence-subband dispersion by the new parameters.

V. MAGNETO-OPTICAL ABSORPTION IN $In_{1-x}Ga_xAs/InP$ STRAINED QUANTUM WELLS

Magneto-optical effects have been widely used to evaluate the reduced effective mass and exciton binding energy of III-V bulk materials and quantum wells.[60–73] Previously, we determined these parameters in lattice-matched $In_{0.53}Ga_{0.47}As/InP$ quantum wells as a function of well width, by analyzing diamagnetic shifts of the ground-state $1S$ electron-HH exciton resonance.[74] Using the well-width-dependent electron effective mass calculated by Eq. (30) with $\alpha=1$ and $\beta=0$, we also evaluated in-plane HH effective mass and valence-band Luttinger-Kohn parameters γ_1 and $\bar\gamma$. In what follows, we study magneto-optical absorption of biaxially strained $In_{1-x}Ga_xAs/InP$ quantum wells on (001) InP substrates, and obtain the effective-mass parameters. In addition to the $1S$ excitons, diagmagnetic shifts of higher-order $2S$ and $3S$ excitons are evaluated.

A. Exciton effective-mass equations under magnetic fields

Under a magnetic field B, perpendicular to quantum-well layers, the exciton resonance energy is written as

$$E_{\rm ex}=E_A+E_{c,n}^z+E_{v,n}^z+E_r+E_{\rm sp}\ , \tag{41}$$

where E_r is given by the effective-mass equation[75]

$$\left[-\frac{\hbar^2}{2\mu}\left[\frac{\partial^2}{\partial r^2}+\frac{1}{r}\frac{\partial}{\partial r}\right]-\frac{e^2}{4\pi\varepsilon\rho}+\frac{e^2B^2}{8\mu}r^2\right]\psi_{\rm env}=E_r\psi_{\rm env}\ , \tag{42}$$

$\mu=(m_e^{\parallel-1}+m_h^{\parallel-1})^{-1}$ is the in-plane reduced effective mass, $m_e^\parallel$ is the in-plane electron effective mass, $m_h^\parallel$ is the in-plane hole effective mass, e is the electron charge, $\mathbf{r}$ is the in-plane distance between an electron and a hole, $\rho=[r^2+(z_e-z_h)^2]^{1/2}$, and ε is the static dielectric constant. The third term on the left in Eq. (42), the diamagnetic energy term, forms parabolic in-plane confinement potentials and increases the exciton energy. The envelope wave function is written as

$$\psi_{\rm env}=\frac{1}{\sqrt{D}}\phi_n^i(\mathbf{r})\varphi_{e,n}(z_e)\varphi_{h,n}(z_h)$$
$$=\frac{1}{D}\sum_{\mathbf{k}_\parallel}A_n^i(\mathbf{k}_\parallel)e^{i\mathbf{k}_\parallel\cdot\mathbf{r}}\varphi_{e,n}(z_e)\varphi_{h,n}(z_h)\ , \quad (43)$$

where $\phi_n^i(\mathbf{r})$ represents the in-plane relative motion of an electron and a hole, $\varphi_{e,n}(z_e)$ is the electron confined-state wave function, $\varphi_{h,n}(z_h)$ is that of a hole, $A_n^i(\mathbf{k}_\parallel)$ is the expansion coefficient by the product of conduction- and valence-band plane waves, and superscript i represents the relative-motion orbital. We neglected mixing in the confined-state wave functions since excitons are formed primarily from band-edge states. We omitted the terms for the in-plane center-of-mass motion and the angular momentum, taking into account the selection rules of optical transitions under the electric-dipole approximation. The spin-splitting energy is $E_{\rm sp}=\pm\mu_B\xi B$ (+ for $M_J=\frac{3}{2}$ and $\frac{1}{2}$ and − for $M_J=-\frac{3}{2}$ and $-\frac{1}{2}$), where $\mu_B=e\hbar/2m_0$, $\xi=g_e/2-3\kappa-27q/4$ for electron-HH excitons, $\xi=\pm g_e/2-\kappa-q/4$ for electron-LH excitons, g_e is the g factor of the conduction-band electron, and κ and q are Luttinger-Kohn valence-band parameters.[5] Since we found no spin splitting of the exciton resonances (see Sec. V B and Refs. 73 and 74), we neglect $E_{\rm sp}$.

To obtain the eigenvalues of Eq. (42), we use the variational approach for 1S-state excitons. For the trial wave function, we take the linear combination of the hydrogenic and harmonic-oscillator wave functions:[71]

$$\phi_n^{1S}(\mathbf{r})=\left[\frac{2}{\pi}\right]^{1/2}\left[\frac{a}{\lambda}e^{-r/\lambda}+\frac{b}{\eta}e^{-r^2/\eta^2}\right], \quad (44)$$

where λ, η, a, and b are variational parameters. Three of them are independent, and are varied to find the combination which minimizes the exciton energy. The Fourier transform of Eq. (44) is

$$A_n^{1S}(\mathbf{k}_\parallel)=\frac{1}{\sqrt{D}}\int d^2\mathbf{r}e^{-i\mathbf{k}_\parallel\cdot\mathbf{r}}\phi_n^{1S}(\mathbf{r})$$
$$=\left[\frac{2\pi}{D}\right]^{1/2}\left[\frac{2\lambda a}{(1+k_\parallel^2\lambda^2)^{3/2}}+\eta b e^{-\eta^2k_\parallel^2/4}\right]. \quad (45)$$

For higher-order S-state excitons, we solve the differential equation, Eq. (42), by the fourth-order Runge-Kutta method.[76]

To include the effect of nonparabolic band dispersion in the calculation, we replace the kinetic-energy term in Eq. (42) with the sum in $\mathbf{k}$ space as

$$\langle\psi_{\rm env}|-\frac{\hbar^2}{2m_e^\parallel}\left[\frac{\partial^2}{\partial r^2}+\frac{1}{r}\frac{\partial}{\partial r}\right]|\psi_{\rm env}\rangle$$
$$=\sum_{\mathbf{k}_\parallel}E_{c,n}^\parallel(\mathbf{k}_\parallel)|A_n^i(\mathbf{k}_\parallel)|^2 \quad (46)$$

and

$$\langle\psi_{\rm env}|-\frac{\hbar^2}{2m_h^\parallel}\left[\frac{\partial^2}{\partial r^2}+\frac{1}{r}\frac{\partial}{\partial r}\right]|\psi_{\rm env}\rangle$$
$$=\sum_{\mathbf{k}_\parallel}E_{v,n}^\parallel(\mathbf{k}_\parallel)|A_n^i(\mathbf{k}_\parallel)|^2\ . \quad (47)$$

By this replacement, we can obtain the in-plane electron effective mass from Eq. (46), the in-plane hole effective mass from Eq. (47), and thus, the reduced effective mass of excitons for a given band dispersion, and calculate E_r as a function of magnetic field. $E_{c,n}^\parallel(\mathbf{k}_\parallel)$ is given by Eq. (33), and $E_{v,n}^\parallel(\mathbf{k}_\parallel)$ by Eq. (40) using Luttinger-Kohn parameters. We can determine the parameters to best describe the exciton resonance diamagnetic shifts.

B. Magneto-optical absorption spectra

We grew multiple quantum wells consisting of $In_{1-x}Ga_xAs$ well layers and InP barrier layers on (001) InP substrates by metalorganic vapor-phase epitaxy. the number of well layers, N, was from 10 to 20. The composition was from $x=0.34$ to 0.58, corresponding to $\varepsilon_\parallel=-0.88$ to $+0.78\%$, and the well width was from $L_w=6$ to 14 nm (Table II). Since these well widths are below Matthews' critical thickness, where misfit dislocations are generated,[77,78] the samples grow coherently on the substrates. The barrier widths L_B are thick enough to neglect the interference of confined-state wave functions between neighboring wells. The growth conditions and the structural evaluation techniques (transmission electron microscope and x-ray diffraction) are described

TABLE II. Composition x, in-plane strain $\varepsilon_\parallel$, well width L_w, barrier width L_B, and splitting energies between 1e-hh and 1e-lh exciton resonances, $\Delta E_{\rm hl}$, of $In_{1-x}Ga_xAs$/InP quantum wells on (001) InP substrates.

Sample	x	$\varepsilon_\parallel(\%)$	L_w (nM)	L_B (nm)	$\Delta E_{\rm hl}$ (meV)
I	0.34	−0.88	7.2	7.6	105±3
II	0.35	−0.81	9.7	9.4	82±3
III	0.42	−0.33	10.1	9.7	49±1
IV	0.46	>0.1	13.6	9.5	14
V	0.47	>0.1	10.0	9.6	22
VI	0.47	>0.1	6.3	9.4	51±3
VII	0.55	0.57	10.0	11.6	−11±2
VIII	0.58	0.78	9.9	11.4	−25±1

in Ref. 74. We also grew a lattice-matched 0.3-μm $In_{0.53}Ga_{0.47}As$ epitaxial layer for magneto-optical measurements.

We focused the light dispersed by a 0.32-m monochrometer perpendicularly to the quantum-well planes and measured the transmitted light intensity as a function of the wavelength. The polarization vector is parallel to the quantum-well layers. We applied the magnetic fields of up to 7–8 T perpendicularly to the samples using a split-coil superconducting magnet at 2 K. The ratio between light intensity transmitted from a sample I_1, and an InP substrate I_2, was normalized to one at an energy below the absorption edge. We calculated the optical absorbance of one quantum well from $\alpha L_{QW} = (1/N)\ln(I_2/I_1)$, where $L_{QW} = L_w + L_B$.

Optical-absorption spectra of three quantum wells at 77 K (Fig. 4) show several exciton resonances. Differences in the strength indicate that resonance at the absorption edge is due to electron-HH excitons (1e-hh) in (a) biaxially compressive and (b) lattice-matched quantum wells, and to electron-LH excitons (1e-lh) in (c) biaxially tensile quantum wells. Under biaxial compression ($x < 0.468$), the splitting between 1e-hh and 1e-lh resonances, ΔE_{hl}, increases from that of the lattice-matched quantum well as x decreases (Fig. 5 and Table II). Under biaxial tensile strain ($x > 0.468$), the positions of 1e-hh and 1e-lh exciton resonances are reversed.

In magneto-optical absorption spectra of biaxially compressive quantum wells [Fig. 6(a)], the ground-state 1e-hh exciton resonance shows diamagnetic shifts, and its strength increases remarkably. This strength enhancement is caused by the shrinkage of the in-plane relative-

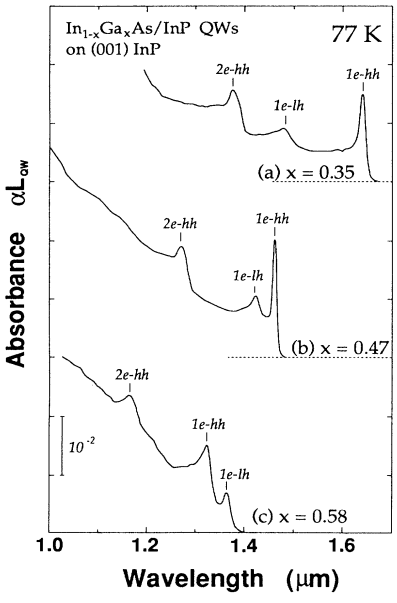

FIG. 4. Optical-absorption spectra of $In_{1-x}Ga_xAs/InP$ quantum wells on (001) InP substrates at 77 K: (a) $x = 0.35$ and $L_w = 9.7$ nm; (b) $x = 0.47$ and $L_w = 10.0$ nm; and (c) $x = 0.58$ and $L_w = 9.9$ nm.

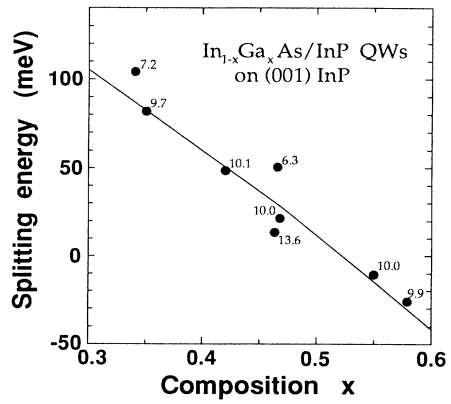

FIG. 5. Splitting between 1e-hh and 1e-lh resonances, ΔE_{hl}, in $In_{1-x}Ga_xAs/InP$ quantum wells on (001) InP substrates. Numbers next to the solid circles are well widths in nm. Solid line is the calculated HH-LH valence-subband splitting for 10-nm quantum wells using $\gamma_1 = 10.8 - 6.6x$ and $\bar{\gamma} = 4.4 - 3.0x$.

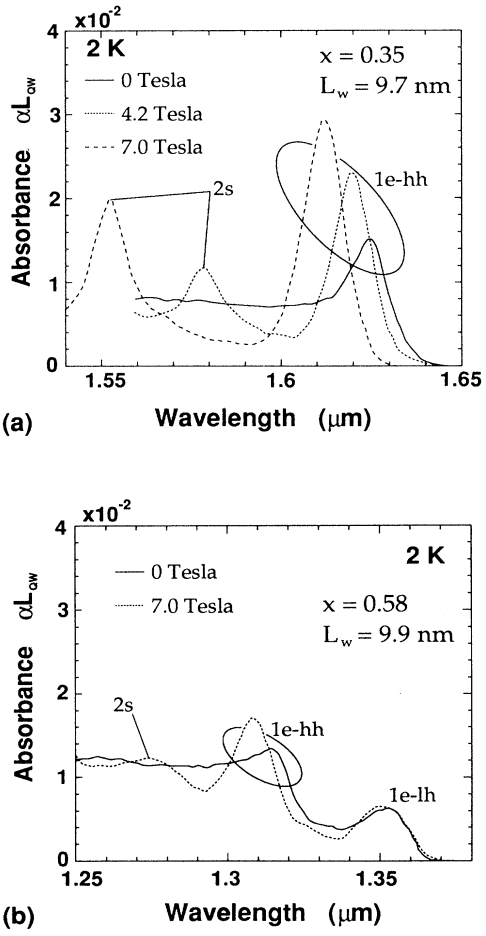

FIG. 6. Magneto-optical absorption spectra at 2 K of $In_{1-x}Ga_xAs/InP$ quantum wells on (001) InP substrates: (a) $x = 0.35$ and $L_w = 9.7$ nm, and (b) $x = 0.58$ and $L_w = 9.9$ nm.

motion wave function under parabolic in-plane confinement potential, proportional to the square of magnetic field.[60,72–74] At the shorter wavelength, a new resonance, which can be attributed to the 1*e*-hh 2*S* exciton resonance, appears and has larger diamagnetic shifts. In a biaxially tensile quantum well [Fig. 6(b)], the spectra of the ground-state 1*e*-lh resonance hardly changes in either energy or strength. Diamagnetic shifts and increase in strength can be seen in the 1*e*-hh exciton resonance at shorter wavelengths, and 2*S* resonance appears. See our previous work (Ref. 74) for magneto-optical absorption spectra of the three lattice-matched quantum wells ($x=0.46-0.47$) in Table II.

In biaxially compressive quantum wells, 1*e*-hh exciton resonance shows diamagnetic shifts of up to 5–6 meV in the measured field region [Fig. 7(a)], and shifts of up to 4–5 meV in the biaxially tensile quantum wells [Fig. 7(b)]. We calculated the lines to best describe the 1*e*-hh diamagnetic shifts by Eq. (42). We used the variational method including conduction-band and valence-band nonparabolicity from Eqs. (46) and (47). We determined the Luttinger-Kohn parameters γ_1 and $\bar{\gamma}$ by the following procedure: First, we calculated the valence-subband edge energies using Eq. (39), with $\mathbf{k}_\parallel=\mathbf{0}$ and found sets of γ_1 and $\bar{\gamma}$ which give the measured splitting energy between the 1*e*-lh and 1*e*-hh resonances. We then found a unique set that describes the 1*e*-hh diamagnetic shifts. We took into account differences in the exciton binding energies between the two resonances. We used a common dielectric constant of $\varepsilon=13.9\varepsilon_0$ for all samples. In-plane reduced, electron, and HH effective masses of 1*S* 1*e*-hh excitons at zero field, and Luttinger-Kohn parameters, are listed in Table III. Masses increased by a few percent as the magnetic field increased due to the magnetic-field-induced extension of $A_1^{1S}(\mathbf{k}_\parallel)$ over nonparabolic dispersion. Values of E_r at zero field, i.e., exciton binding energy E_b are also listed in Table III.

Figure 7(b) also includes the calculated diamagnetic shifts of the ground-state 1*e*-lh exciton resonance in the tensile-strain samples using the determined Luttinger-Kohn parameters. The in-plane reduced, electron, and LH effective masses are $\mu=0.051m_0$, $m_e^\parallel=0.051m_0$, and $m_{\rm lh}^\parallel=-4.8m_0$ for $x=0.58$; and $\mu=0.067m_0$, $m_e^\parallel=0.051m_0$, and $m_{\rm lh}^\parallel=-0.22m_0$ for $x=0.55$. The negative LH effective mass is due to the repulsion from

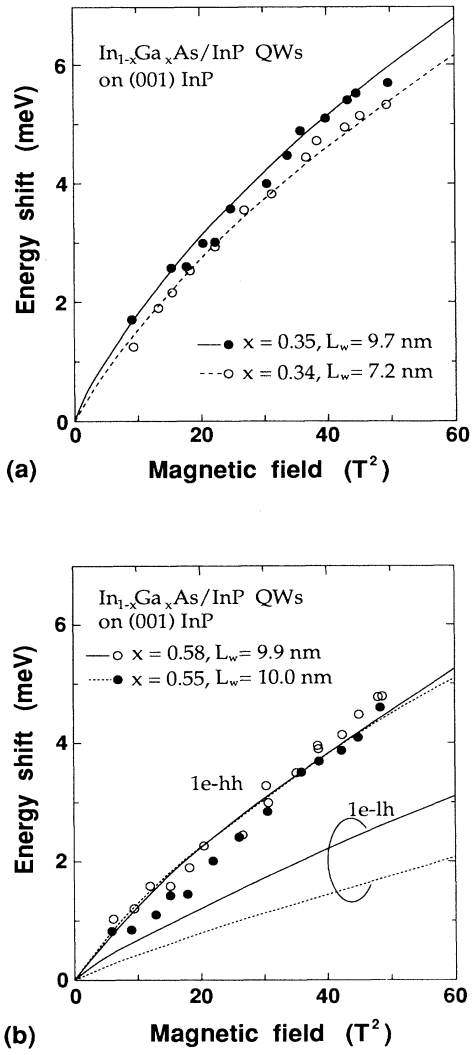

FIG. 7. Diamagnetic shifts of the 1*e*-hh 1*S* exciton resonance spectra (solid and open circles) as a function of the square of the magnetic field in (001) $In_{1-x}Ga_xAs/InP$ quantum wells: (a) under biaxially compressive strain, and (b) under biaxially tensile strain. Lines are calculated for 1*e*-hh and 1*e*-lh resonances which best fit the experimental results using γ_1 and $\bar{\gamma}$ as parameters (Table III).

TABLE III. Parameters of 1*e*-hh excitons at zero field; in-plane reduced effective mass μ, in-plane electron effective mass $m_e^\parallel$, in-plane heavy-hole effective mass $m_{\rm hh}^\parallel$, and binding energy E_b. Effective masses are in units of m_0. γ_1 and $\bar{\gamma}$ are Luttinger-Kohn parameters. n.m. stands for "not measured."

Sample	μ	$m_e^\parallel$	$m_{\rm hh}^\parallel$	E_b (meV)	γ_1	$\bar{\gamma}$
I	0.033	0.050	0.099	−6.2	9.4	3.6
II	0.032	0.047	0.099	−5.7	9.1	3.2
III	n.m.	n.m.	n.m.	n.m.	n.m.	n.m.
IV	0.037	0.048	0.15	−5.8	5.8	2.0
V	0.035	0.05	0.12	−6.1	8.1	2.4
VI	0.04	0.054	0.16	−7.3	6.3	2.5
VII	0.039	0.051	0.17	−6.4	7.6	3.4
VIII	0.038	0.051	0.15	−6.4	7.8	2.9

lower HH subbands, making the reduced effective mass larger, and diamagnetic shifts smaller, than in the 1e-hh excitons. Though we did not plot the diamagnetic shifts of 1e-hh exciton resonance, because of the large uncertainties of the resonance energy in the weak and broad spectra, it is clear in Fig. 6(b) that 1e-lh resonance has smaller shifts than 1e-hh.

We plotted the 1e-hh exciton resonance energies, including higher-order 2S and 3S resonances, as a function of the magnetic field in Fig. 8. In calculating the diamagnetic shifts of 2S and 3S states by Eq. (42), we assumed a parabolic band and used the zero-field effective masses obtained for 1S excitons (Table III). Though slight deviations are observed in the high-magnetic-field region, presumably due to nonparabolic band dispersion, the calculation agrees well with measurements. The dashed lines are Landau fans calculated using the zero-field reduced effective mass and the exciton binding energy (Table III). Note that we must take into account Coulomb interaction, even in higher-order resonances.

We measured magneto-optical absorption (solid circles) for bulk lattice-matched $In_{0.53}Ga_{0.47}As$ (Fig. 9). The solid lines are the calculated diamagnetic shifts of electron-HH excitons, and dashed lines are the shifts of electron-LH excitons. We replaced the kinetic-energy operator for two-dimensions in Eq. (42) with that for three dimensions and solved the equation by the Runge-Kutta method assuming parabolic dispersion. Averaging Luttinger-Kohn parameters for the three lattice-matched quantum wells (Table III), we obtain $\gamma_1=6.7$ and $\bar{\gamma}=2.3$, and a bulk band-edge effective mass of $m_0/(\gamma_1-2\bar{\gamma})=0.48m_0$ for the HH band and

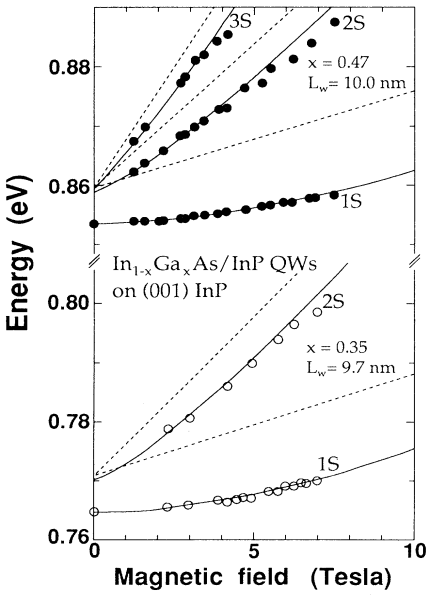

FIG. 8. Diamagnetic shifts of 1S, 2S, and 3S 1e-hh exciton resonances for lattice-matched ($x=0.47$ and $L_w=10.0$ nm) and biaxially compressive ($x=0.35$ and $L_w=9.7$ nm) (001) $In_{1-x}Ga_xAs$/InP quantum wells. Solid lines are calculated from Eq. (42) and dashed lines are Landau fans.

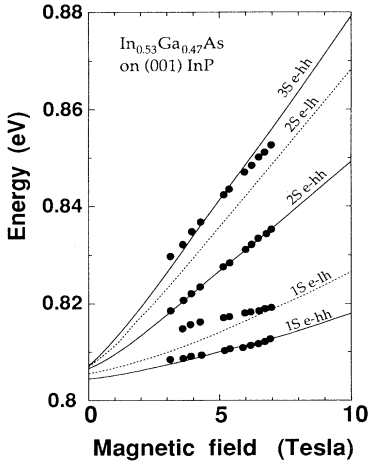

FIG. 9. Exciton diamagnetic shifts in lattice-matched $In_{0.53}Ga_{0.47}As$ on a (001) InP substrate. Solid lines are the calculated S-state electron-HH exciton resonance, and dashed lines are the S-state electron-LH resonance.

$m_0/(\gamma_1+2\bar{\gamma})=0.088m_0$ for the LH band. Using $\mu=0.040m_0$ for the HH band, and $\mu=0.029m_0$ for the LH band ($m_e=0.044m_0$), the calculation agrees well with measurements.

We plotted the integrated intensity of 1e-hh exciton resonance spectra as a function of magnetic field [Fig. 10(a)]. Lines are calculated using the magnetic-field dependence of the expansion coefficient [Eq. (45)], and the wave-vector-dependent matrix element including the momentum matrix element P^2 (see Ref. 74 for details of the calculation). We determined P^2 to best describe the measured integrated intensity. The magnetic-field-induced enhancement of the integrated intensity is a result of the extension of the expansion coefficients in $\mathbf{k}_\parallel$ space [shrinkage of $\phi_1^{1S}(r)$ in real space]. We plotted the matrix elements determined by this procedure, m_0P^2, for both compressive and lattice-matched quantum wells [Fig. 10(b)]. Equation (26), based on the first-order $\mathbf{k}\cdot\mathbf{p}$ perturbation ($D'=0$), underestimates the matrix element by about 20% (solid line). The dashed line, assuming $D'=-6$, explains well the measured matrix element for both lattice-matched and compressive quantum wells. This shows that Eq. (26) describes the momentum matrix element, independent of strain, at least up to a strain of about 1%. This supports the validity of our calculation of the conduction-band-edge effective mass in Fig. 3.

We plotted the in-plane effective-mass parameters of 1S 1e-hh excitons at zero field for quantum wells of about 10 nm [Figs. 11(a) and 11(b)]. The solid line [Fig. 11(a)] represents the band-edge electron effective mass from the second derivative of $E_{c,n}^{\parallel}(\mathbf{k}_\parallel)$ [Eq. (33)] for a 10-nm-wide well. The electron effective mass of excitons is a few percent larger than the band-edge mass because of the extension of the exciton expansion coefficient in $\mathbf{k}_\parallel$ space in a nonparabolic band. The error bars in the in-plane HH effective mass correspond to $\pm5\%$ uncertainty in the calculated electron effective mass. The HH masses are 2–3 times larger than the electron masses. Note that the HH

masses are a few tens of a percent larger than those of diagonal terms of the Luttinger-Kohn Hamiltonian, $(\gamma_1+\bar{\gamma})^{-1}$, due to the nonparabolic dispersion under intersubband mixing. The reduced effective mass increases with the composition due to the increase in both the electron and hole masses.

We plotted Luttinger-Kohn parameters for all samples [Fig. 11(c)]. Error bars are about ± 1 in γ_1 and ± 0.1 in $\bar{\gamma}$ if we assume $\pm 5\%$ error in the calculated electron effective mass. The solid lines are plotted by multiplying Lawaetz's calculations (linear interpolation between InAs and GaAs) by 0.55 for γ_1 and by 0.5 for $\bar{\gamma}$ (the least-square fit); $\gamma_1 = 10.8 - 6.6x$ and $\bar{\gamma} = 4.4 - 3.0x$. Note that these values explain well the HH and LH splitting energies (solid line in Fig. 5). The values (almost half) significantly modify the calculated in-plane valence-band dispersion through changes in the mass of Eq. (34) diagonal terms: $(m_0/(\gamma_1+\bar{\gamma})$ for HH and $m_0/(\gamma_1-\bar{\gamma})$ for LH, and the change in the degree of intersubband mixing which depends on the splitting energies and the magnitude of nondiagonal terms. To calculate Luttinger-Kohn parameters, we need the interband momentum matrix elements and the energy separations between valence-band edges and remote even-parity band edges. The uncertainties in these quantities, which can hardly be ob-

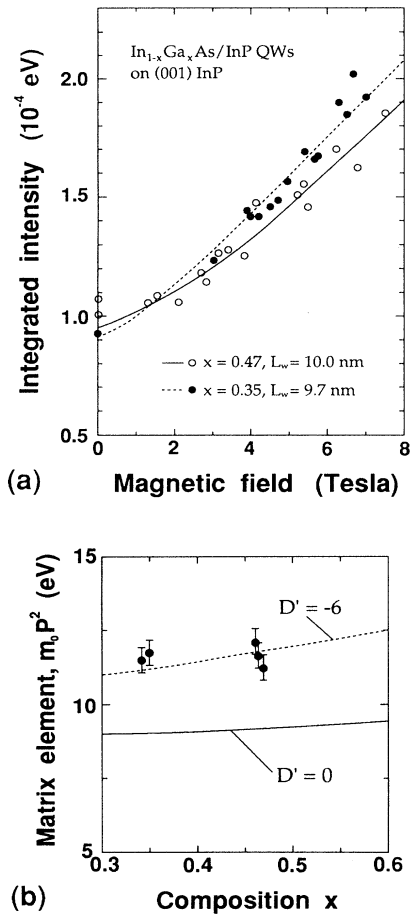

FIG. 10. (a) Integrated intensity of the 1*e*-hh 1*S* exciton resonance spectra as a function of magnetic field. (b) Momentum matrix element m_0P^2. The solid line is calculated from Eq. (26) with $D'=0$, and the dashed line with $D'=-6$.

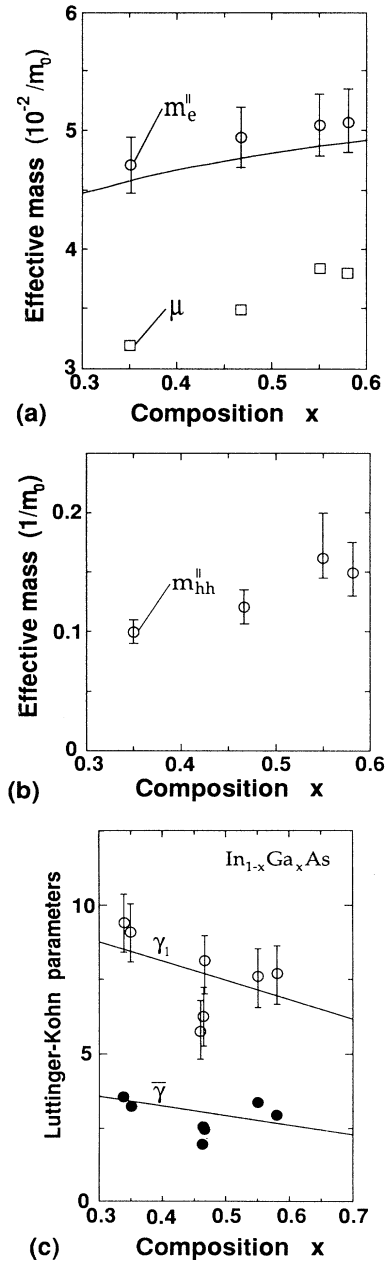

FIG. 11. (a) In-plane electron and reduced effective masses of 1*e*-hh 1*S* excitons at a zero field in (001) $In_{1-x}Ga_xAs/InP$ quantum wells with a well width of approximately 10 nm. Solid line is the calculated band-edge electron effective mass from Eq. (30) for a 10-nm well width. (b) In-plane HH effective mass of 1*e*-hh 1*S* excitons at a zero field in (001) $In_{1-x}Ga_xAs/InP$ quantum wells with a well width of approximately 10 nm. (c) Luttinger-Kohn valence-band parameters γ_1 and $\bar{\gamma}$ in $In_{1-x}Ga_xAs$. Solid lines are plotted by multiplying Lawaetz's calculations by 0.55 for γ_1 and by 0.5 for $\bar{\gamma}$: $\gamma_1 = 10.8 - 6.6x$ and $\bar{\gamma} = 4.4 - 3.0x$.

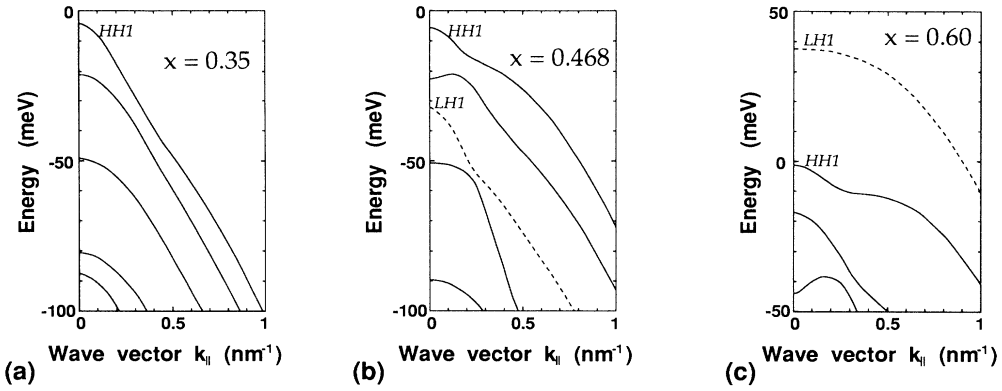

FIG. 12. Calculated in-plane valence-subband dispersion for (a) biaxially compressive ($x=0.35$), (b) lattice-matched ($x=0.468$), and (c) biaxially tensile ($x=0.6$) $In_{1-x}Ga_xAs/InP$ quantum wells with 10-nm well width on (001) InP substrates.

tained experimentally, may explain the discrepancy between Lawaetz's calculations and our values.

We calculated the in-plane valence-subband dispersion of (001) $In_{1-x}Ga_xAs/InP$ quantum wells with 10-nm well width using our experimentally determined Luttinger-Kohn parameters (Fig. 12): (a) $x=0.35$ ($\gamma_1=8.5$ and $\bar{\gamma}=3.4$); (b) $x=0.468$ ($\gamma_1=7.7$ and $\bar{\gamma}=3.0$); and (c) $x=0.6$ ($\gamma_1=6.8$ and $\bar{\gamma}=2.6$). Though detail structures, such as effective masses, subband splitting energies, and nonparabolicity, are markedly changed by new parameters, qualitative features are preserved (compare the results with Fig. 7 of Ref. 27); subbands are highly nonparabolic due to intersubband mixing in lattice-matched quantum wells. Under compressive strain, the large HH-LH splitting reduces the mixing, resulting in rather parabolic dispersion. Under tension, the LH1 band is the ground state and has heavy in-plane effective mass. The HH1 band has a lower effective mass than the LH1, making the $1e$-hh exciton diamagnetic shifts larger, as in Fig. 7(b).

VI. CONCLUSION

We studied conduction- and valence-band structures in $In_{1-x}Ga_xAs/InP$ strained quantum wells on (001) InP substrates by the $\mathbf{k}\cdot\mathbf{p}$ perturbation approach and magneto-optical absorption of exciton resonances. We derived a formula for calculating conduction-band dispersion both in biaxially strained bulk materials and quantum wells based on the first-order $\mathbf{k}\cdot\mathbf{p}$ perturbation approach. We use our formula to show that the electron effective mass of strained $In_{1-x}Ga_xAs$ and strained $In_{1-x}Ga_xAs/InP$ quantum wells are anisotropic, and that the masses depend significantly on the strain and well width. By analyzing the magneto-optical absorption spectra of electron-HH exciton resonance, we obtained in-plane electron, hole, and reduced effective masses of excitons, and Luttinger-Kohn effective-mass parameters for valence bands as a function of composition. We clarified quantitatively both conduction- and valence-band structures of (001) $In_{1-x}Ga_xAs/InP$ quantum wells.

APPENDIX A

Using the Slater-Koster list,[48] the interatomic matrix elements of zinc-blende crystals are given by

$$E_{x,x}=V_{pp\sigma}/3+2V_{pp\pi}/3 \tag{A1}$$

and

$$E_{x,yz}=V_{pd\sigma}/3-2\sqrt{3}V_{pd\pi}/9\ . \tag{A2}$$

From Harrison's table,[48] we have

$$V_{pp\sigma}=3.24\frac{\hbar^2}{m_0d^2}\ , \tag{A3}$$

$$V_{pp\pi}=-0.81\frac{\hbar^2}{m_0d^2}\ , \tag{A4}$$

$$V_{pd\sigma}=-2.95\frac{\hbar^2r_d^{3/2}}{m_0d^{7/2}}\ , \tag{A5}$$

and

$$V_{pd\pi}=1.36\frac{\hbar^2r_d^{3/2}}{m_0d^{7/2}}\ , \tag{A6}$$

where d is the interatomic distance, r_d is the d-orbital radius, $\hbar$ is Planck's constant divided by 2π, and m_0 is the electron mass.

APPENDIX B

The orbital-strain Hamiltonian given by Bir and Pikus[16,17] is

$$\begin{aligned}H_\varepsilon=&-a_s(\varepsilon_{xx}+\varepsilon_{yy}+\varepsilon_{zz})\\&-3b_s\left[\left[L_x^2-\frac{L^2}{3}\right]\varepsilon_{xx}+\text{c.p.}\right]\\&-\sqrt{3}d_s[(L_xL_y+L_yL_x)\varepsilon_{xy}+\text{c.p.}]\ ,\end{aligned} \tag{B1}$$

where ε_{ij} are the components of the strain tensor; L and L_x are the angular-momentum operators; c.p. is the cyclic permutation with respect to the indices x, y, and z; a_s

is the hydrostatic deformation potential; and b_s and d_s are the uniaxial deformation potentials. For valence bands, using the six band-edge bases to diagonalize spin-orbit interaction [Eqs. (9)–(14)], the matrix of (B1) with the diagonal spin-orbit splitting energy Δ is given by

$$H_\varepsilon = -\begin{array}{c} \begin{matrix} |\frac{3}{2},\frac{3}{2}\rangle & |\frac{3}{2},\frac{1}{2}\rangle & |\frac{3}{2},-\frac{1}{2}\rangle & |\frac{3}{2},-\frac{3}{2}\rangle & |\frac{1}{2},\frac{1}{2}\rangle & |\frac{1}{2},-\frac{1}{2}\rangle \end{matrix} \\ \begin{bmatrix} P_\varepsilon+Q_\varepsilon & -S_\varepsilon & R_\varepsilon & 0 & \frac{1}{\sqrt{2}}S_\varepsilon & -\sqrt{2}R_\varepsilon \\ -S_\varepsilon^* & P_\varepsilon-Q_\varepsilon & 0 & R_\varepsilon & \sqrt{2}Q_\varepsilon & -\sqrt{\frac{3}{2}}S_\varepsilon \\ R_\varepsilon^* & 0 & P_\varepsilon-Q_\varepsilon & S_\varepsilon & -\sqrt{\frac{3}{2}}S_\varepsilon^* & -\sqrt{2}Q_\varepsilon \\ 0 & R_\varepsilon^* & S_\varepsilon^* & P_\varepsilon+Q_\varepsilon & \sqrt{2}R_\varepsilon^* & \frac{1}{\sqrt{2}}S_\varepsilon^* \\ \frac{1}{\sqrt{2}}S_\varepsilon^* & \sqrt{2}Q_\varepsilon & -\sqrt{\frac{3}{2}}S_\varepsilon & \sqrt{2}R_\varepsilon & P_\varepsilon+\Delta & 0 \\ -\sqrt{2}R_\varepsilon^* & -\sqrt{\frac{3}{2}}S_\varepsilon^* & -\sqrt{2}Q_\varepsilon & \frac{1}{\sqrt{2}}S_\varepsilon & 0 & P_\varepsilon+\Delta \end{bmatrix} \end{array}, \tag{B2}$$

where

$$P_\varepsilon = a_s(\varepsilon_{xx}+\varepsilon_{yy}+\varepsilon_{zz}) , \tag{B3}$$

$$Q_\varepsilon = \frac{b_s}{2}(2\varepsilon_{zz}-\varepsilon_{xx}-\varepsilon_{yy}) , \tag{B4}$$

$$S_\varepsilon = -(\varepsilon_{zx}-i\varepsilon_{yz})d_s , \tag{B5}$$

$$R_\varepsilon = \frac{\sqrt{3}}{2}b_s(\varepsilon_{xx}-\varepsilon_{yy})-id_s\varepsilon_{xy} . \tag{B6}$$

Assuming that epitaxial layers are grown coherently on substrates, the crystal lattices distort tetragonally and have biaxial strain. The strain tensor components for (001) epitaxial layers are then $\varepsilon_{xx}=\varepsilon_{yy}=\varepsilon_\parallel$, $\varepsilon_{xy}=\varepsilon_{yz}=\varepsilon_{zx}=0$, $\varepsilon_{zz}=-(2C_{12}/C_{11})\varepsilon_\parallel$, and

$$\varepsilon_\parallel = (a_{\rm sub}-a_0)/a_0 , \tag{B7}$$

where $a_{\rm sub}$ is the lattice constant of the substrate and a_0 is that of the free-standing epitaxial layers. The matrix elements then reduce to

$$P_\varepsilon = 2a_s[(C_{11}-C_{12})/C_{11}]\varepsilon_\parallel , \tag{B8}$$

$$Q_\varepsilon = -b_s[(C_{11}+2C_{12})/C_{11}]\varepsilon_\parallel , \tag{B9}$$

and

$$S_\varepsilon = R_\varepsilon = 0 . \tag{B10}$$

Note that $|\frac{3}{2},\pm\frac{1}{2}\rangle$ and $|\frac{1}{2},\pm\frac{1}{2}\rangle$ states intermix because of the nondiagonal uniaxial strain terms. The eigenvalues of Eq. (B2) are[4]

$$E_{\rm HH} = -P_\varepsilon - Q_\varepsilon \tag{B11}$$

for $|\frac{3}{2},\pm\frac{3}{2}\rangle$ HH states,

$$E_{\rm LH} = -P_\varepsilon + \tfrac{1}{2}(Q_\varepsilon - \Delta + \sqrt{\Delta^2+2\Delta Q_\varepsilon+9Q_\varepsilon^2}) \tag{B12}$$

for $|\frac{3}{2},\pm\frac{1}{2}\rangle$ LH states, and

$$E_{\rm SO} = -P_\varepsilon + \tfrac{1}{2}(Q_\varepsilon - \Delta - \sqrt{\Delta^2+2\Delta Q_\varepsilon+9Q_\varepsilon^2}) \tag{B13}$$

for $|\frac{1}{2},\pm\frac{1}{2}\rangle$ split-off states. The eigenstates for coupled LH and split-off states are[4,54,55]

$$f_{\rm LH}^{\pm} = \alpha|\tfrac{3}{2},\pm\tfrac{1}{2}\rangle + \beta|\tfrac{1}{2},\pm\tfrac{1}{2}\rangle \tag{B14}$$

and

$$f_{\rm SO}^{\pm} = -\beta|\tfrac{3}{2},\pm\tfrac{1}{2}\rangle + \alpha|\tfrac{1}{2},\pm\tfrac{1}{2}\rangle , \tag{B15}$$

where

$$\alpha = \frac{2\sqrt{2}|Q_\varepsilon|}{C} , \tag{B16}$$

$$\beta = \frac{(A-B)|Q_\varepsilon|}{CQ_\varepsilon} , \tag{B17}$$

$$A = \Delta + Q_\varepsilon , \tag{B18}$$

$$B = \sqrt{\Delta^2+2Q_\varepsilon\Delta+9Q_\varepsilon^2} , \tag{B19}$$

and

$$C = \sqrt{2B(B-A)} . \tag{B20}$$

α and β represent the degree of mixing and satisfy the normalizing condition of $|\alpha|^2+|\beta|^2=1$.

The conduction band, using s-state basis functions [Eq. (8)], shifts by[4]

$$P_\varepsilon^c = 2a_c[(C_{11}-C_{12})/C_{11}]\varepsilon_\parallel , \tag{B21}$$

where a_c is the conduction-band hydrostatic deformation potential.

[1]R. Hull and J. C. Bean, *Semiconductors and Semimetals* (Academic, New York, 1991), Vol. 33, Chap. 1.
[2]S. T. Picraux, B. L. Doyle, and J. Y. Tsao, *Semiconductors and Semimetals* (Academic, New York, 1991), Vol. 33, Chap. 3.
[3]W. J. Schaff, P. J. Tasker, M. C. Foisy, and L. F. Eastman, *Semiconductors and Semimetals* (Academic, New York, 1991), Vol. 33, Chap. 2.
[4]F. H. Pollak, *Semiconductors and Semimetals* (Academic, New York, 1990), Vol. 32, Chap. 2.
[5]J. M. Luttinger and W. Kohn, Phys. Rev. **97**, 869 (1955).
[6]S. S. Nedorezov, Fiz. Tverd. Tela (Leningrad) **12**, 2269 (1971) [Sov. Phys. Solid State **12**, 1814 (1971)].
[7]Y.-C. Chang and J. N. Schulman, Appl. Phys. Lett. **43**, 536 (1983).
[8]M. Altarelli, J. Lumin. **30**, 472 (1985).
[9]G. Bastard and J. A. Brum, IEEE J. Quantum Electron. **QE-22**, 1625 (1986).
[10]Y.-C. Chang, Appl. Phys. Lett. **46**, 710 (1986).
[11]R. Eppenga, M. F. H. Schuurmans, and S. Colak, Phys. Rev. B **36**, 1554 (1987).
[12]M. Altarelli, U. Ekenberg, and A. Fasolino, Phys. Rev. B **32**, 5138 (1985).
[13]S. Colak, R. Eppenga, and M. F. H. Schuurmans, IEEE J. Quantum. Electron. **QE-23**, 960 (1987).
[14]D. Ahn, S. L. Chuang, and Y.-C. Chang, J. Appl. Phys. **64**, 4056 (1988).
[15]D. Ahn and S. L. Chuang, IEEE J. Quantum. Electron. **QE-26**, 13 (1990).
[16]G. L. Bir and G. E. Pikus, *Symmetry and Strain-Induced Effects in Semiconductors* (Wiley, New York, 1974).
[17]G. E. Pikus and G. L. Bir, Fiz. Tverd. Tela (Leningrad) **1**, 1642 (1959) [Sov. Phys. Solid State **1**, 1502 (1959)].
[18]J. C. Hensel and G. Ficher, Phys. Rev. **129**, 1041 (1963).
[19]E. P. O'Reilly and G. P. Witchlow, Phys. Rev. B **34**, 6030 (1986).
[20]E. Yablonovitch and E. O. Kane, IEEE J. Lightwave Technol. **LT-4**, 504 (1986).
[21]E. P. O'Reilly, K. C. Heasman, A. R. Adams, and G. P. Witchlow, Supuerlatt. Microstruct. **3**, 99 (1987).
[22]E. Yablonovitch and E. O. Kane, IEEE J. Lightwave Technol. **LT-6**, 1202 (1988).
[23]L. C. Andreani, A. Pasquarello, and F. Bassani, Phys. Rev. B **36**, 5887 (1987).
[24]E. P. O'Reilly, Semicond. Sci. Technol. **4**, 121 (1989).
[25]T. C. Chong and C. G. Fonstad, IEEE J. Quantum. Electron. **QE-25**, 171 (1989).
[26]S. L. Chuang, Phys. Rev. B **43**, 9649 (1991).
[27]C. Y.-P. Chao and S. L. Chuang, Phys. Rev. B **46**, 4110 (1992).
[28]I. Suemune, L. A. Coldren, M. Yamanishi, and Y. Kan, Appl. Phys. Lett. **53**, 1378 (1988).
[29]T. Ohtoshi and N. Chinone, IEEE Photon. Tech. Lett. **1**, 117 (1989).
[30]A. R. Adams, Electron. Lett. **22**, 249 (1986).
[31]M. Sugawara, Appl. Phys. Lett. **60**, 1842 (1992).
[32]P. J. A. Thijs, J. J. M. Binsma, L. F. Tiemeijer, and T. van Dongen (unpublished).
[33]L. F. Tiemeijer, P. J. A. Thijs, P. J. de Waard, J. J. J. M. Binsma, and T. van Dongen, Appl. Phys. Lett. **58**, 2738 (1991).
[34]P. J. A. Thijs, J. J. M. Binsma, E. W. A. Young, and W. M. E. Van Gils, Electron. Lett. **27**, 791 (1991).
[35]P. J. A. Thijs, L. F. Tiemeijer, P. I. Kuindersma, J. J. M. Binsma, and T. van Dongen, IEEE J. Quantum Electron. **QE-27**, 1426 (1991).
[36]P. Lawaetz, Phys. Rev. B **4**, 3460 (1971).
[37]M. Sugawara, Phys. Rev. B **47**, 7588 (1993).
[38]G. Bastard, J. A. Brum, and R. Ferreira, in *Solid State Physics,* edited by H. Ehrenreich and D. Turnbull (Academic, New York, 1991), Vol. 44, p. 229.
[39]S. R. Forrest, P. H. Schmidt, R. B. Wilson, and M. L. Kaplan, Appl. Phys. Lett. **45**, 1199 (1984).
[40]H. Okumura, S. Misawa, S. Yoshida, and S. Gonda, Appl. Phys. Lett. **46**, 377 (1985).
[41]J. Batey and S. L. Wright, J. Appl. Phys. **59**, 200 (1986).
[42]R. E. Cavicchi, D. V. Lang, D. Gershoni, A. M. Sergent, J. M. Vendenberg, S. N. G. Chu, and M. B. Panish, Appl. Phys. Lett. **54**, 739 (1989).
[43]W. A. Harrison, J. Vac. Sci. Technol. **14**, 1016 (1977).
[44]W. A. Harrison, J. Vac. Sci. Technol. B **3**, 1231 (1985).
[45]S. Gonda, Appl. Phys. **55**, 570 (1986) (in Japanese).
[46]S. H. Wei and A. Zunger, Phys. Rev. Lett. **59**, 144 (1987).
[47]S. H. Wei and A. Zunger, Phys. Rev. B **37**, 8958 (1988).
[48]W. A. Harrison, *Electronic Structure and Properties of Solids—The Physics of Chemical Bonds* (Freeman, San Francisco, 1980).
[49]H. Nagai, S. Adach, and T. Fukui, *III-V Alloy Semiconductors* (Corona, Tokyo, 1988), p. 60 (in Japanese).
[50]R. People, K. W. Wecht, K. Alavi, and A. Y. Cho, Appl. Phys. Lett. **54**, 1457 (1989).
[51]D. Gershoni, H. Temkin, J. M. Vandenberg, S. N. G. Chu, R. A. Hamm, and M. B. Panish, Phys. Rev. Lett. **60**, 448 (1988).
[52]E. O. Kane, J. Phys. Chem. Solids **1**, 249 (1957).
[53]E. O. Kane, J. Phys. Chem. Solids **1**, 82 (1956).
[54]H. Hasegawa, Phys. Rev. **129**, 1029 (1963).
[55]L. D. Laude, F. H. Pollak, and M. Cardona, Phys. Rev. B **3**, 2623 (1971).
[56]D. A. Broido and L. J. Sham, Phys. Rev. B **31**, 888 (1985).
[57]A. T. Twardowski and C. Hermann, Phys. Rev. B **35**, 8144 (1987).
[58]M. Altarelli, U. Ekenberg, and A. Fasolino, Phys. Rev. B **32**, 5138 (1985).
[59]U. Ekenberg, L. C. Andreani, and A. Pasquarello, Phys. Rev. B **46**, 2625 (1992).
[60]O. Akimoto and H. Hasegawa, J. Phys. Soc. Jpn. **22**, 181 (1967).
[61]N. Miura, Y. Iwasa, S. Tarucha, and H. Okamoto, in *Proceedings of the 17th International Conference on the Physics of Semiconductors,* edited by J. D. Chadi and W. A. Harrison (Springer, New York, 1984), p. 359.
[62]J. C. Maan, G. Belle, A. Fasolino, M. Altarelli, and K. Ploog, Phys. Rev. B **30**, 2253 (1984).
[63]S. Tarucha, H. Okamoto, Y. Iwasa, and N. Miura, Solid State Commun. **52**, 815 (1984).
[64]S. Tarucha, H. Iwamura, T. Saku, H. Okamoto, Y. Iwasa, and N. Miura, Surf. Sci. **174**, 194 (1986).
[65]D. C. Rogers, J. Singleton, R. J. Nicholas, C. T. Foxon, and K. Woodbridge, Phys. Rev. B **34**, 4002 (1986).
[66]W. Ossau, B. Jakel, E. Bangert, G. Landwehr, and G. Weimann, Surf. Sci. **174**, 188 (1986).
[67]D. J. Mowbray, J. Singleton, M. S. Skolnic, N. J. Pulsford, S. J. Bass, L. L. Taylor, R. J. Nicholas, and W. Hayes, Superlatt. Microstruct. **3**, 471 (1987).
[68]A. S. Plaut, J. Singleton, R. J. Nicholas, R. T. Harley, S. R. Andrews, and C. T. B. Foxon, Phys. Rev. B **38**, 1323 (1988).
[69]D. D. Smith, M. Dutta, X. C. Liu, A. F. Terzis, A. Petrou, M. W. Cole, and P. G. Newman, Surf. Sci. **228**, 184 (1990).
[70]R. J. Warburton, G. M. Sundaram, R. J. Nicholas, S. K. Haywood, G. J. Ress, N. J. Mason, and P. J. Walker, Surf. Sci. **228**, 270 (1990).

[71]X. L. Zheng, D. Heiman, and B. Lax, Phys. Rev. B **40**, 10 523 (1989).
[72]G. E. W. Bauer and T. Ando, Phys. Rev. B **38**, 6015 (1988).
[73]M. Sugawara, Phys. Rev. B **45**, 11 423 (1992).
[74]M. Sugawara, N. Okazaki, T. Fujii, and S. Yamazaki, Phys. Rev. B (to be published).
[75]R. S. Knox, *Theory of Excitons* (Academic, New York, 1963).
[76]K. Sakurai, *Introduction to Quantum Mechanics by Personal Computers* (Syhokaboh, Tokyo, 1989) (in Japanese).
[77]J. W. Matthews and A. E. Blakeslee, J. Vac. Sci. Technol. B **6**, 1285 (1976).
[78]M. Tacano, Y. Sugiyama, and Y. Takeuchi, Appl. Phys. Lett. **58**, 2420 (1991).